Multi-Objective Optimization of Extrusion Parameters for High-Performance Honeycomb Cordierite Ceramics via Orthogonal Design

Xianpeng Huang , Na Wei * , Fengshuang Wang , Xiaoli Zhang *

Posted Date: 25 November 2025

doi: 10.20944/preprints202511.1884.v1

Keywords: cordierite ceramics; extrusion; orthogonal design; mechanical properties; thermal shock resistance

Article

Multi-Objective Optimization of Extrusion Parameters for High-Performance Honeycomb Cordierite Ceramics via Orthogonal Design

Xianpeng Huang [2], Na Wei [1,2,*], Fengshuang Wang [1] and Xiaoli Zhang [1,*]

[1] Weichai Power Co., Ltd., Weifang 261061, China

[2] College of Materials Science and Engineering, Shandong University of Science and Technology, Qingdao 266590, China

* Correspondence: weina@sdust.edu.cn (N.W.); zhangxiaoli@weichai.com (X.Z.)

Abstract

Cordierite diesel particulate filters (DPFs) were prepared using pure cordierit powder with organic binders, sodium silicate aids and pore formers by extrusion technique. The orthogonal test method was adopted to investigate the optimal value of the multi-objective and multi-factor problems. Based on results from statistical analysis, sintering temperature is the most important factor. The optimal parameters included a 3 h holding time, 10 wt.% pore former, 12 wt.% sintering aid, and a sintering temperature of 1150 °C. As the sodium silicate liquid increased and viscosity decreased with the increasing of temperature, which led to the formation of glass phases and the improvement of density. Therefore, with increasing sintering temperature, the porosity and coefficient of thermal expansion decreased. Both the mechanical properties and chemical stability of the prepared samples are strengthened. When the sintering temperature was 1150 °C, the prepared samples with high porosity (67.82%), compressive strength (5.88 MPa), bending strength (13.10 MPa), low thermal expansion coefficient (CTE, 1.82×10^{-6}/°C) showed the best comprehensive performance of thermal shock resistance and filtration efficiency. These results demonstrate great potential for DPF applications and provide a refrence for the design of other honeycomb ceramics with optimum level of liquid phase.

Keywords: cordierite ceramics; extrusion; orthogonal design; mechanical properties; thermal shock resistance

1. Introduction

The exhaust from diesel engines contains a number of air pollutants, including carbon monoxide (CO), hydrocarbons (C_xH_y), nitrogen oxides (NO_x), sulfur oxides (SO_x) and particulate, which is harmful for human health and environmental safety [1,2]. The diesel particulate filter (DPF) has been developed as an efficient solution for trapping and eliminating soot [3]. The filter operates via a honeycomb ceramic wall that features an interconnected porous network. This structure allows exhaust gases to pass through while trapping soot particles, thereby enhancing filtration performance [4]. As worldwide government regulations associated with particulate matter and NOx emissions continue to become increasingly stringent, the more effective filter to satisfy the particulate controlling requirement is imposed [5]. Filter material is an important factor in determining the performance of the DPF system. Cordierite ($2MgO{\cdot}2Al_2O_3{\cdot}5SiO_2$) has received much attention during the past decades as a potential material for the application in DPF, mainly because of its excellent low thermal expansion coefficient, stability at high temperature, high mechanical strength and low cost [6–8]. However, it is still a great challenge to prepare honeycomb cordierite ceramic with high performance of mechanical and thermal properties.

 doi:10.20944/preprints202511.1884.v1

As we all know, even at stoichiometric cordierite compositions, intermediate phases (impurity crystals and amorphous phase) tend to form at relatively low temperatures [9–11], especially when solid-state reaction routes are used for cordierite synthesis. Therefore, the sintering conditions and composition of the cordierite body need to be properly controlled to produce a low-CTE honeycomb. Among the preparation methods, extrusion method is traditionally used to manufacture honeycomb ceramics. The honeycomb ceramics fabricated by extrusion process have high porosity, straight-through channels and readily controllable pore structures [12–14]. Especially, the extrusion method can ensure high production of honeycomb ceramics with low cost. However, during the preparation process, there are high requirements for the viscosity and plasticity of the mud material. Additionally, many influencing factors in this process, such as the content of pore-forming agents, the content of additives, powder particle size, sintering temperature, and holding time can affect the preparation of materials[15–18]. In generally, an exhaustive research method is used to study every factor effect on properties of materials. To efficiently optimize these variables, the orthogonal test method has been adopted. Based on orthogonal design and mathematical analysis, this approach significantly shortens the experimental cycle and facilitates the development of high-performance new materials [19,20].

In this study, honeycomb cordierite ceramics were fabricated by extrusion using a mixture of commercial cordierite powder (to avoid intermediate phase formation), hydroxypropyl methylcellulose, polyvinyl alcohol, sodium silicate (as a sintering aid), and carbon powder (as a pore-forming agent). The fluidity of sodium silicate facilitates its homogeneous distribution around powder particles, thereby enhancing sintering. An orthogonal experimental design was applied to optimize four key parameters: sintering temperature, holding time, pore-forming agent content, and sintering aid content. The optimal parameter combination was successfully identified. Furthermore, the effect of sintering temperature on pore structure, mechanical properties, thermal shock resistance, and filtration performance was systematically investigated.

2. Materials and Methods

2.1. Raw Material

Cordierite ($2MgO{\cdot}2Al_2O_3{\cdot}5SiO_2$) powders with a particle size of d_{50}=45 μm (Jiangxi Henghao New Material Technology Co., Ltd, China) are commercially available. The purity of cordierite is over 97% according to the supplier's information. Carbon powders (C, Fuchen Tianjin Chemical Reagent Co., Ltd, China) were used as pore-forming agent. Hydroxypropyl methylcellulose (HPMC, Tianjin Huasheng Chemical Reagent, China), Glycerol ($C_3H_8O_3$, Tianjin Fuyu Fine Chemicals, China), sodium silicate (Na_2SiO_3, Aladdin Reagent Co., Ltd, China) and polyvinyl alcohol (PVA, Aladdin Reagent Co., Ltd., China) were also used.

2.2. Preparation of Honeycomb Shaped Cordierite

Cordierite powder was mixed with carbon powder (0–15 wt%) for 0.5 h, followed by addition of sodium silicate (6–15 wt.%) as a sintering aid. A binder of 5 wt.% aqueous PVA solution (based on total powder mass) was introduced, along with 8 wt.% HPMC, 32 wt.% deionized water, and 5 wt.% glycerol (relative to cordierite mass). The mixture was kneaded for 0.5 h to form homogeneous clay, then processed in a vacuum pug mill to remove air bubbles and impurities. After aging in a sealed container for 48 h, the clay was shaped by extrusion. The dried samples were sintered at 1000–1300 °C for 1–4 h to obtain honeycomb cordierite ceramics. The preparation process was shown in Figure 1.

 doi:10.20944/preprints202511.1884.v1

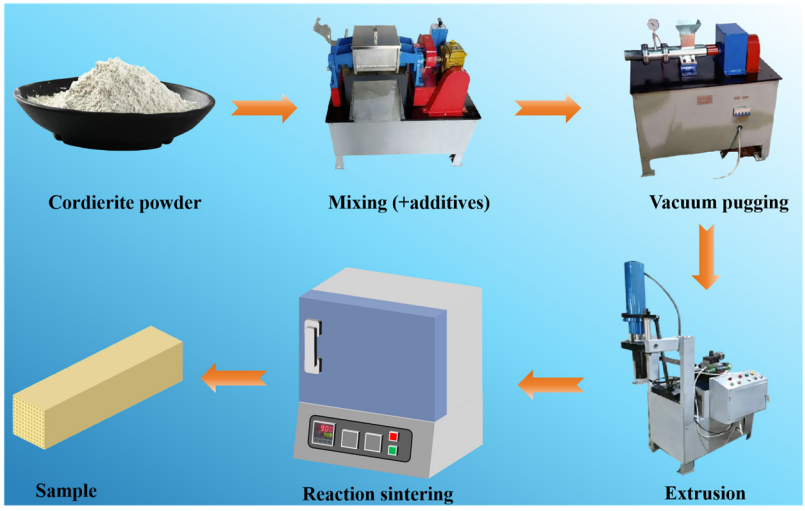

Figure 1. Schematic of extrusion molding method for fabrication of honeycomb shaped cordierite ceramics.

2.3. Orthogonal Experimental Design (OED)

The OED is an effective mathematical method for multi-factor experimental design, which can fully explore the interaction relationships between different factors and their levels within a limited number of trials. Its characteristics include uniform and independent level settings for each experimental factor, ensuring that every level of each factor is thoroughly examined across all trials, thereby avoiding errors caused by factor cross-interference. In the research, four factors, including sintering temperature (A), holding time (B), pore-forming agent content (C), and sintering aid content (D) were selected to the orthogonal design factors and each factor was selected in four levels. Factors and levels for orthogonal test design were shown in Table 1.

Table 1. Factor and level table.

Level	Factor level			
	Sintering temperature (°C)	Holding time (h)	Pore-forming agent content (wt.%)	Sintering aid content (wt.%)
	A	B	C	D
1	800	1	0	6
2	900	2	5	9
3	1000	3	10	12
4	1150	4	15	15

2.4. Characterization

The phase compositions of the as-prepared samples were analyzed by X-ray diffraction (XRD). The morphology of fractured surface was obtained by scanning electron microscopy (SEM, NANO450, FEI). Open porosity was measured by the Archimedes method. A mercury intrusion porosimeter (Micromeritics AutoPore V 9600) was used to analyze the pore size distribution. Compressive strength was evaluated on 20 mm × 20 mm × 20 mm samples with an MTS E45.305 universal testing machine. Bending strength was measured by the three-point bending method on an INSTRON-5582 testing machine. The CTE was evaluated from room temperature to 800 °C using a thermal dilatometer (ZRPY-1400).

The thermal shock resistance was assessed based on the methods stipulated in standards JC/T 2396-2017 and GB/T 25994-2010. Samples with size of 40mm×40mm×100mm were subjected to thermal cycling in a muffle furnace at 650 °C for 30min, followed by rapid removal and natural cooling to room temperature. Cycling was continued until crack initiation was observed on the

 doi:10.20944/preprints202511.1884.v1

honeycomb walls. Chemical stability was assessed by measuring the mass loss after corrosion in acidic and alkaline solution. Prior to testing, all samples were ultrasonically cleaned and oven-dried to a constant mass (M_1). The samples were then subjected to immersion in 20 vol.% H_2SO_4 and 1 vol.% NaOH solutions at 80 °C for 1 h, respectively. Subsequently, the samples were dried and weighed (M_2). The mass loss rate (R) was calculated according to the equation of $R=(M_1-M_2)/M_1\times100\%$. A gravimetric method was employed to determine the filtration efficiency of cordierite samples against carbon aerosol. Briefly, 0.05 g of carbon powder was dispersed in anhydrous ethanol to form a 2000 ppm stock solution. Prior to testing, each cordierite sample was dried at 110 °C for 10 h and its initial mass (M_0) was recorded. The sample was then installed in the home-made test apparatus, and the carbon black aerosol was generated by injecting the solution into an atomizer, with a nitrogen carrier gas flow set at 100 mL/min. After the test, the sample was dried thoroughly to remove the ethanol and weighed again (M_1). The mass gain ($\Delta M_1=M_1-M_0$) represents the mass of captured carbon black. Additionally, the carbon aerosol was dried thoroughly to remove the ethanol and weighed again (M_3). The mass loss of the carbon powder was ΔM_2 (ΔM_2=0.05g-M3). The filtration efficiency (η) was calculated using the following formula of $\eta=(\Delta M_1/\Delta M_2)\times100\%$.

3. Results

3.1. Orthogonal Test Results

According to the predetermined factors and levels, an L_{16} Taguchi orthogonal array was adopted to investigate the effects of these factors on the pore structure and properties of cordierite ceramics. To evaluate the influence of different factor levels, porosity, compressive strength, and thermal shock resistance were measured, as summarized in Table 2. The effects of various factors on these properties were assessed and the optimal combination of factor levels was determined using range analysis. Table 3 provides the range analysis of this orthogonal experiment, in which K_i (level i = 1, 2, 3, 4) and R are important parameters. K_i is defined as the average value of the test performance at the four levels of the corresponding factor, and R is defined as the difference between the K_{max} and K_{min} values in the corresponding factor column. For example, for porosity, when the factor A is 1 (800 °C), K_1 = (76.46 + 72.98 + 61.2 +58.94)/4, R = max{67.40, 65.23, 66.26, 59.72}− min{67.40, 65.23, 66.26, 59.72} = 7.68. By comparing the K values, the optimal level for each factor can be identified. The R value reflects the fluctuation range of the K values, thus, a larger R value indicates a more significant influence of that factor on the experimental results [21,22].

In Table 3, it can be found that the greatest influence on porosity was holding time, followed by sintering temperature, sintering aid content, and pore-forming agent content, namely B>A>D>C. By observing the maximum values of K_1, K_2, K_3 and K_4, the optimal combination of process parameters were A1 (800 °C), B_1 (1 h), C_4 (15 wt.%) and D_1 (6wt.%). The sintering temperature was the biggest influence on the compressive strength, followed by pore-forming agent content, holding time, and sintering aid content, that is A>B>C>D. It should be noted that for compressive strength, the optimal parameters were A_4 (1150 °C), B_2 (2 h), C_1 (0 wt.%) and D_4 (15 wt.%). The four factors affecting thermal shock resistance were ranked in descending order of influence: sintering temperature, pore-forming agent content, holding time, and sintering aid content, that is A>C>B=D. To sum up, the main factor affects the compressive strength and thermal shock resistance is the sintering temperature. For thermal shocks, the optimal parameters were A_4 (1150 °C), B_3 (3 h), C_2 (5 wt.%) and D_3 (12 wt.%).

Figure 2 is drawn according to the K values of the porosity, compressive strength, and thermal shock resistance in Table 3. As shown in Figure 2a, the porosity of the samples decreased gradually with the increase in sintering temperature and the extension of holding time, which can be attributed to the enhanced density of the samples. Moreover, a higher content of sodium silicate as the sintering aid promoted the formation of a liquid phase, which not only filled the pores but also facilitated particle rearrangement and densification. Consequently, the overall porosity decreased significantly. In contrast, porosity exhibited an increasing trend as the content of the pore-forming agent rises. Figure 2b reveals a negative correlation between compressive strength and porosity. Meanwhile, as

 doi:10.20944/preprints202511.1884.v1

illustrated in Figure 2c, the thermal shock resistance improved notably with increasing sintering temperature. The maximum thermal shock resistance was achieved at a sintering temperature of 1150 °C. However, beyond this point, cracks began to appear after three thermal cycles.

Taking into account the influencing factors and parameters of various properties, it can be seen from the factors affecting thermal shock resistance and compressive strength that sintering temperature is the main influencing factor. And, the effect of sintering temperature on microstructure and properties was investigated in the following research. The holding time was set to 3 h, as it represents the optimal level for thermal shock resistance. Analysis of the optimal parameters for compressive strength and thermal shock resistance reveals that when the pore-forming agent content increases from 0 wt.% to 5 wt.%, the thermal shock resistance improves. This indicates that introducing a small number of pores can significantly enhance thermal shock resistance without a notable increase in overall porosity. Accordingly, a pore-forming agent content of 10 wt.% was selected to balance porosity requirements, even though the thermal shock resistance may slightly decrease at this level. In addition, a sintering aid content of 12 wt.% was identified as the optimal value for thermal shock resistance. Based on these considerations, the final optimized combination of process parameters was determined as follows: holding time of 3 h, pore-forming agent content of 10 wt.%, and sintering aid content of 12 wt.%.

Table 2. The design and results of orthogonal table of L16(4^4).

No.	Factors				Porosity (%)	Compressive strength (MPa)	Thermal shock cycles
	A	B	C	D			
1	800	1	0	6	76.46	0.20	2
2	900	1	5	9	69.45	0.25	2
3	1000	1	10	12	71.29	0.45	2
4	1150	1	15	15	69.27	2.38	3
5	800	2	10	9	72.98	0.23	2
6	900	2	15	6	73.22	0.72	1
7	1000	2	0	15	60.01	1.42	3
8	1150	2	5	12	57.24	3.17	4
9	800	3	15	12	61.20	0.26	2
10	900	3	10	15	56.91	0.46	2
11	1000	3	5	6	63.92	0.82	3
12	1150	3	0	9	51.79	3.09	3
13	800	4	5	15	58.94	0.45	2
14	900	4	0	12	61.34	0.75	2
15	1000	4	15	9	69.83	0.81	2
16	1150	4	10	6	60.58	2.52	2

Table 3. Range analysis of properties of cordierite ceramics obtained based on orthogonal test.

	Parameter	A	B	C	D
Porosity (%)	K_1	67.40	71.62	62.40	68.55
	K_2	65.23	65.86	62.39	66.01
	K_3	66.26	58.46	65.44	62.77
	K_4	59.72	62.67	68.38	61.28
	R	7.68	13.16	5.99	7.27
Compressive strength (MPa)	K_1	0.28	0.82	1.36	1.06
	K_2	0.54	1.38	1.17	1.09
	K_3	0.88	1.16	0.92	1.16
	K_4	2.70	1.13	1.04	1.18
	R	2.42	0.56	0.44	0.12
	K_1	2	2.25	2.5	2

 doi:10.20944/preprints202511.1884.v1

Thermal shock cycles	K_2	1.75	2.5	2.75	2.25
	K_3	2.5	2.5	2	2.5
	K_4	3	2	2	2.5
	R	1.25	0.5	0.75	0.5

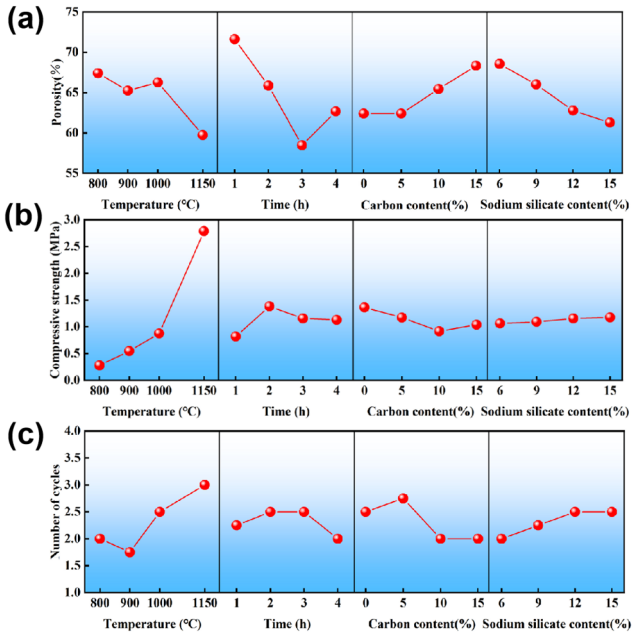

Figure 2. Influence of four factors on the (a) Porosity, (b) Compressive strength and (c) thermal shock resistance.

3.2. Effects of Sintering Temperature

Figure 3 shows the XRD patterns of samples sintered at different temperatures, in which all diffraction peaks were indexed to cordierite (PDF#82-1887). As the sintering temperature increased, a gradual weakening of the cordierite diffraction peaks was observed, which could be attributed to the growth of an amorphous phase. At 1000 °C, the viscous sodium silicate liquid reacted only minimally with cordierite, preserving most of the crystalline grains and resulting in the highest peak intensity [23]. When the temperature rised to 1150 °C, the increased fluidity of the liquid phase promoted the dissolution of cordierite, forming a thicker glassy layer that significantly raised the amorphous fraction and further weakened the diffraction peaks. As the temperature reached 1300 °C, the highly fluid liquid induced extensive dissolution, penetrating even into the grain interiors. This process maximized the volume of the glassy phase and led to the lowest intensity of the crystalline cordierite peaks.

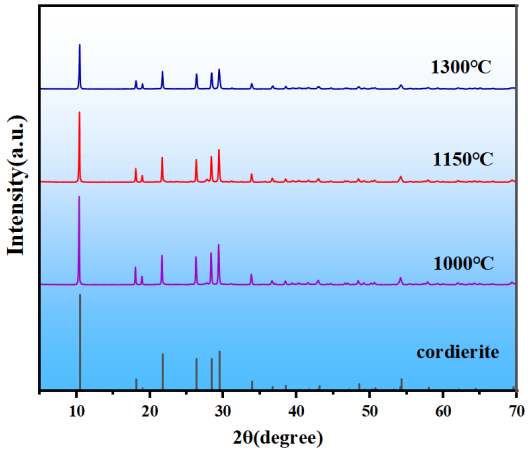

 doi:10.20944/preprints202511.1884.v1

Figure 3. XRD patterns of samples sintered at 1000 °C, 1150 °C and 1300 °C.

Figure 4 shows the SEM images of samples sintered at different temperatures. The prepared cordierite ceramics presented three-dimensional interconnected pore structure. As shown in Figures 4a and 4b, when the temperature was 1000oC, the particles were mainly in point contact, and the sintered sample showed a loose structure. With the sintering temperature increased, the sintered neck became more and more obvious (Figures 4c and 4d). However, when the temperature reached to 1300oC, the surface of the particles was bonded by a large amount of liquid phase, the pores were significantly reduced, and the density was increased.

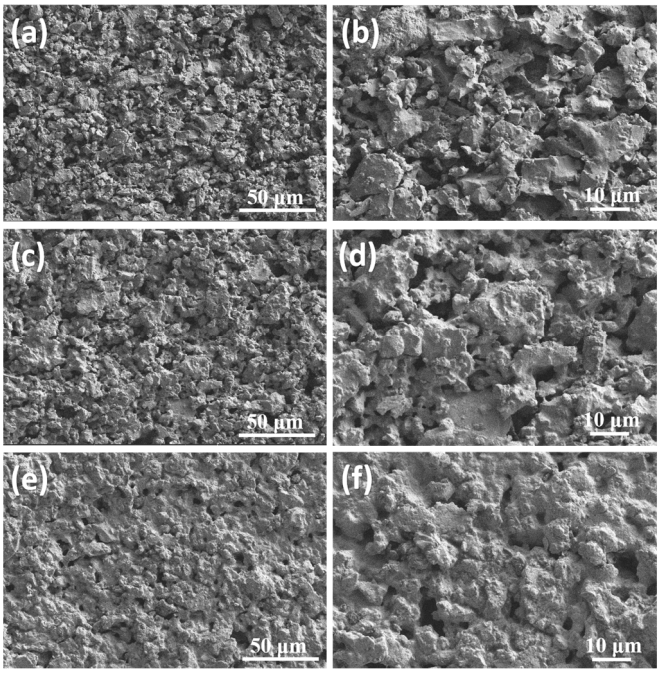

Figure 4. SEM images of samples sintered at different temperatures. (a) 1000 °C, (b) 1150 °C and (c) 1300 °C.

The pore structure develops in three key stages. Initially, between room temperature and 600 °C, organics and carbonaceous substances decomposed, releasing gaseous products and creating an interconnected open-pore network, which established the high porosity of the green body. Subsequently, between 600 °C and 1150 °C, molten sodium silicate formed a wetting liquid phase. A reaction at the cordierite–liquid interface produced a glassy phase that bonds adjacent particles [24]. Finally, during the high-temperature holding stage, the sintering mechanism became strongly temperature-dependent. At 1000 °C, viscous flow induced particle rearrangement, resulting in a weak, highly porous structure. As the temperature rises to 1150 °C, a less viscous liquid facilitated a dissolution–precipitation process, promoting strong interparticle connections and forming a robust porous network. In contrast, at 1300 °C, solid-state sintering combined with liquid volatilization led to over-sintering, resulting in pore closure and a sharp decrease in porosity.

The shrinkage rate exhibited a linear increase trend with the rise in sintering temperature, which was negative to the trend of the open porosity (Figure 5a). This correlation stems from the nature of the sintering process, which inherently involves densification and volume reduction. Prior to sintering, the gaps between particles in the honeycomb ceramic support were predominantly open pores. As the sintering temperature increased, a liquid phase formed, progressively filling these open pores and leading to pore closure, thereby inducing shrinkage of the ceramic structure. With further temperature increase, the volume of the liquid phase expanded, intensifying the shrinkage. As shown in Figure 5b, when the sintering temperature was raised from 1000 °C to 1150 °C, the open porosity of the cordierite ceramics decreased gradually from 73.00% to 67.82%, which can be attributed to the growing amount of liquid phase promoting the closure of interconnected pores [25]. However, when the temperature reached 1300 °C, the porosity dropped sharply to 22.17% at 1300 °C as decreasing

 doi:10.20944/preprints202511.1884.v1

liquid viscosity accelerated small size of pore elimination, consistented with pore size distribution results (Figure 5c). And the average pore size increased from 3.42 to 4.67 μm as the sintering temperature increased from 1000 to 1300 °C. This result was in accordance with the above SEM analysis.

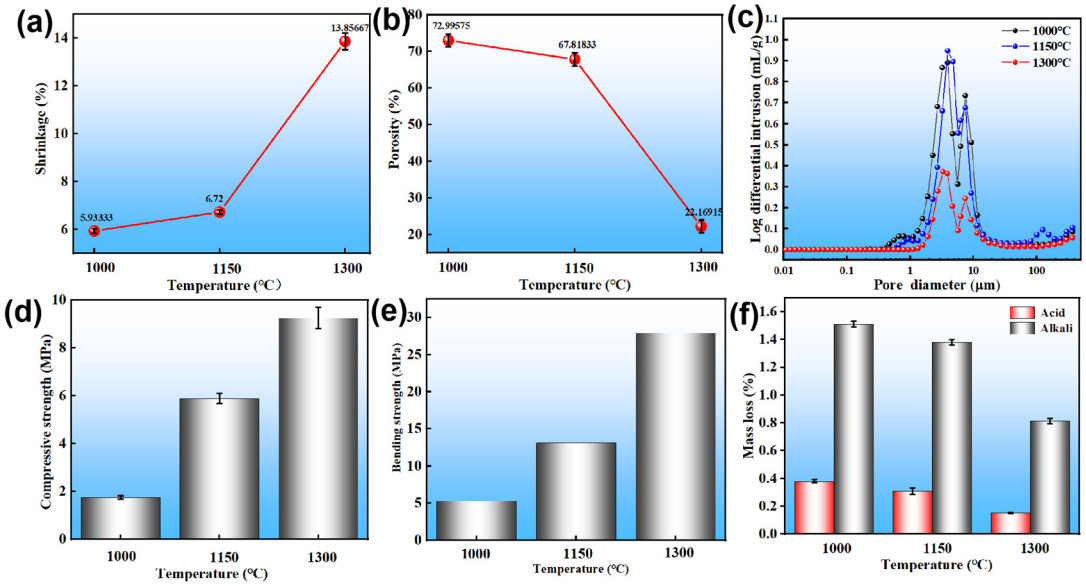

Figure 5. The pore structure and properties of the samples sintered at different temperatures. (a) Shrinkage, (b) Porosity, (c) Pore size distribution, (d) Compressive strength, (e) Bending strength and (f) Corrosion resistance.

Figures 5d and 5e show the compressive strength and flexural strength of the prepared samples, respectively. Both properties increased almost linearly with rising sintering temperature. Specifically, the compressive strengths of samples sintered at 1000 °C, 1150 °C, and 1300 °C were 1.75 MPa, 5.88 MPa, and 9.25 MPa, respectively, while the corresponding bending strengths were 5.27 MPa, 13.10 MPa, and 27.90 MPa. This enhancement in mechanical strength is attributed to the reduction of pores within the ceramic body, which is consistent with the earlier observed decrease in open porosity.

As shown in Figure 5f, the results indicated that the corrosion rate decreased with increasing sintering temperature, which was primarily attributed to a reduction in porosity of the as-prepared samples. Furthermore, the mass loss was consistently more severe in the alkaline solution than that in the acidic solution. This difference stems from the aggressive reaction of OH^- ions with the SiO_2 network in the silicate structure, which generates soluble silicates and leads to widespread dissolution [26]. In contrast, the cordierite structure remained relatively stable in H_2SO_4, owing to its lower susceptibility to attack by H+ ions [27,28].

As the shown in Figure 6a, the CTE increased from 1.13×10^{-6}/°C to 2.82×10^{-6}/°C with increasing sintering temperatures. The CTE of cordierite ceramics stemed mainly from the glassy and cordierite phases. With the increasing of sintering temperature, the high fraction of glassy phases resulted in the relatively higher CTE values. Furthermore, the presence of an amorphous phase not only increased the CTE but also can induce thermal stress cracking when DPFs were exposed to the rapid thermal cycles of vehicle exhaust systems [29]. In Figure 6b, the honeycomb ceramic sintered at 1150 °C exhibited optimal thermal shock resistance, sustaining 8 cycles before crack initiation, whereas the sample sintered at 1000 °C failed after only 5 cycles. The inferior performance at 1000 °C was due to weak interparticle bonding, which offered low resistance to thermal stress. Conversely, the sample sintering at 1150 °C promoted the formation of a reinforcing glass phase that created strong necks between particles, thereby enhancing fracture strength. The decline in performance at 1300 °C was ascribed to an increased thermal expansion coefficient [30]. Figure 6c shows the schematic diagram of filtration device. As illustrated in the Figure 6d, the filtration efficiency of carbon black particles exhibited an negative correlation with the sintering temperature. A maximum efficiency of 97.27%

 doi:10.20944/preprints202511.1884.v1

was achieved at 1150 °C. This decline was attributed to the concomitant reduction in porosity and specific surface area, coupled with an increase in average pore diameter.

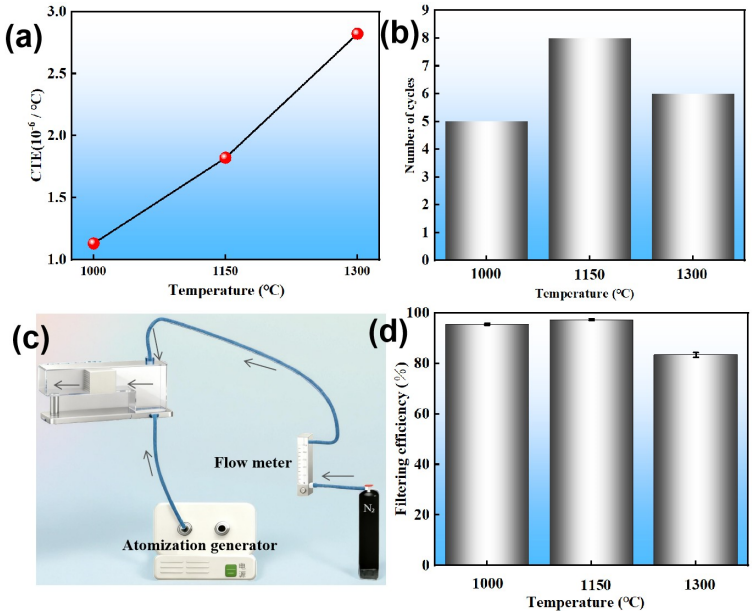

Figure 6. The CTE (a), thermal shock resistance (b), schematic diagram of filtration device (c) and filtering efficiency (d) of the samples sintered at different temperatures.

4. Conclusions

In conclusion, honeycomb cordierite ceramics were fabricated by extrusion and optimized using an L16 (4^4) orthogonal experiment. Sintering temperature was identified as the most significant factor, with the optimal parameters determined as 3 h holding time, 10 wt.% pore-forming agent, and 12 wt.% sintering aid. Further investigation into sintering temperature revealed that as temperature increased from 1000 °C to 1300 °C, porosity decreased sharply from 73.00% to 22.17%, which was attributed to enhanced liquid phase formation and pore coalescence. This densification led to improved mechanical properties. In addition, the mechanical properties and chemical stability of the prepared samples are strengthened with increasing sintering temperature. The sample sintered at 1150 °C with low coefficient of thermal expansion (1.82×10^{-6}/°C) achieved an optimal balance, exhibiting excellent thermal shock resistance and high filtration performance.

Author Contributions: Conceptualization, N.W and X.H.; methodology, N.W and X.H.; validation, N.W and X.H.; formal analysis, N. W; investigation, N.W and X.H.; data curation, N.W and X.H.; writing—original draft preparation, N. W; writing—review and editing, N.W, F.W. and X.Z.; supervision, N.W, F.W. and X.Z.; funding acquisition, N.W. All authors have read and agreed to the published version of the manuscript.

Funding: This research was funded by the Shandong Province Postdoctoral Innovation Project (No. SDCX-ZG-202303086), China Postdoctoral Science Foundation (2023M732677); and Key Program of National Natural Science Foundation of China (52331004).

Institutional Review Board Statement: Not applicable.

Data Availability Statement: Data will be available on request.

Conflicts of Interest: The author declares that there are no conflicts of interest.

 doi:10.20944/preprints202511.1884.v1

References

1. Khanna, S., Dewangan, A.K., Yadav, A.K., Ahmad, A. A progressive review on strategies to reduce exhaust emissions from diesel engine: Current trends and future options. *Environ. Prog. Sustain.* **2025**, *44*, e70012.
2. Zhang, C., Gao, S., Yu, D., Zhou, S., Wang, L., Yu, X., Zhao, Z. Research progress on preparation of cerium-based oxide catalysts with specific morphology and their application for purification of diesel engine exhaust. *J. Rare Earth.* **2024**, *42*, 1187-1216.
3. Zhang, Z., Dong, R., Lan, G., Yuan, T., Tan, D. Diesel particulate filter regeneration mechanism of modern automobile engines and methods of reducing PM emissions: A review. *Environ. Sci. Pollut. R.* **2023**, *30*, 39338-39376.
4. Liu, Z., Huang, S., Song, J., Dong, S., Pan, T., Zhang, Y., Wang, K., Liu, Y., Preparation and mechanism study of pin rod SiC reinforced cordierite-based diesel particulate filters. *J. Eur. Ceram. Soc.* **2025**, *45*, 117135.
5. Meng, Z., Wang, W., Zeng, B., Bao, Z., Hu, Y., Ou, J., Liu, J., An experimental investigation of particulate emission characteristics of catalytic diesel particulate filters during passive regeneration. *Chem. Eng. J.* **2023**, *468*, 143549.
6. An, D., Wang, L., Liu, X., Zhang, Y., Liang, J., Meng, J., Preparation and properties of cordierite-based multi-phase composite far-infrared emission ceramics by fine-grained tailings. *Ceram. Int.* **2024**, *50*, 29729-29737.
7. Appiah, M., Yang, Y., Ullah, B., Xiao, Y., Tan, D.Q., Exceptionally optimized millimeter-wave properties of cordierite-based materials via innovative processing and predictive analytics. *J. Eur. Ceram. Soc.* **2025**, *45*, 117206.
8. Shyam, A., Bruno, G., Watkins, T.R., Pandey, A., Lara-Curzio, E., Parish, C.M., Stafford, R.J., The effect of porosity and microcracking on the thermomechanical properties of cordierite. *J. Eur. Ceram. Soc.* **2015**, *35*, 4557-4566.
9. Li, S., Bao, C., Dong, W. and Liu, R., Phase evolution and properties of porous cordierite ceramics prepared by cordierite precursor pastes based on supportless stereolithography. *J. Alloy. Compound.* **2022**, *922*, 166295.
10. Wang, H., Wang, S., Meng, Z., Chen, Z., Liu, L., Wang, X., Qian, D. and Xing, Y., Mechanism of cordierite formation obtained by high temperature sintering technique. *Ceram. Int.*, **2023**, *49*, 20544-20555.
11. Wahsh, M.M.S., Mansour, T.S., Othman, A.G.M., Bakr, I.M. Recycling bagasse and rice hulls ash as a pore-forming agent in the fabrication of cordierite-spinel porous ceramics. *Int. J. Appl. Ceram. Tec.* **2022**, *19*, 2664-2674.
12. Elbadawi, M., Wally, Z.J. and Reaney, I.M. Porous hydroxyapatite-bioactive glass hybrid scaffolds fabricated via ceramic honeycomb extrusion. *J. Am. Ceram. Soc.* **2018**, *101*, 3541-3556.
13. Wang, W., Li, Z., Gao, X., Huang, Y., He, R. Material extrusion 3D printing of large-scale SiC honeycomb metastructure for ultra-broadband and high temperature electromagnetic wave absorption. *Addit. Manuf.* **2024**, *85*, 104158.
14. Huang, X., Ma, C., Sun, T., Yu, Y., Wu, Y., Wu, Y., Zang, G., Fu, J., Yu, C., Liu, X., Jiang, B. A novel honeycomb ceramic for gas treatment prepared by microarc oxidation. *Ceram. Int.*, **2025**, *51*, 12525-12533.
15. Isobe, T., Tomita, T., Kameshima, Y., Nakajima, A., Okada, K. Preparation and properties of porous alumina ceramics with oriented cylindrical pores produced by an extrusion method. *J. Eur. Ceram. Soc.* **2006**, *26*, 957-960.
16. Nurhudan, A.I., Supriadi, S., Whulanza, Y., Saragih, A.S. Additive manufacturing of metallic based on extrusion process: A review. *J. Manuf. Process.* **2021**, *66*, 228-237.
17. Guo, X., Cai, X., Zhu, L., Zhang, L., Yang, H. Preparation and properties of SiC honeycomb ceramics by pressureless sintering technology. *J. Adv. Ceram.* **2014**, *3*, 83-88.
18. Li, Z., Zhou, W., Zhou, Z., Sun, N., Liu, Y., Liu, W., Yang, X., Pui, D.Y. Microwave drying coupled with convective air and steam for efficient dehydration of extruded zeolite honeycomb monolith. *Ceram. Int.*, **2024**, *50*, 43674-43682.
19. Yin, Y., Li, A., Wu, D., Li, J., Guo, J. Low-resistance optimization and secondary flow analysis of elbows via a combination of orthogonal experiment design and simple comparison design. *Build. Environ.* **2023**, *236*, 110263.

 doi:10.20944/preprints202511.1884.v1

20. Zhong, B., Zhou, X., Gu, Q., Ding, J., Zhang, C., Zhu, H., Wang, Z. Orthogonal design of bioinspired butterfly-wing microstructures for enhanced anti-reflection performance. *Opt. Laser Technol.* **2025**, *192*, 113840.
21. Wang, S., Xiang, Y., Feng, H., Cui, Y., Liu, X., Chang, X., Guo, J. and Tu, P. Optimization of 3D printing parameters for alumina ceramic based on the orthogonal test. *ACS omega* **2024**, *9*,16734-16742.
22. Kang, P., Zhao, Q., Guo, S., Xue, W., Liu, H., Chao, Z., Jiang, L. and Wu, G. Optimisation of the spark plasma sintering process for high volume fraction SiCp/Al composites by orthogonal experimental design. *Ceram. Int.*, **2021**, *47*, 3816-3825.
23. Zhou, Y., Zhu, D., Zhang, X., Liang, J. Effect of spontaneous polarization of tourmaline on the grain growth behavior of 3YSZ powder. *J. Am. Ceram. Soc.* **2022**, *105*, 4542-4553.
24. Jiang, Q., Xie, Y., Ji, L., Zhong, Z., Xing, W. Low-temperature sintering of a porous SiC ceramic filter using water glass and zirconia as sintering aids. *Ceram. Int.* **2021**, *47*, 26125-26133.
25. Sürel, M.Ş. and Topateş, G.Ü.L.S.Ü.M. Role of liquidus temperature and composition on the densification and properties of cordierite. *Ceram. Int.* **2025**, *51*, 34016–34024.
26. Wu, J., Hu, C., Pi, C., Xu, X. and Xiang, W. Preparation and corrosion resistance of cordierite-spodumene composite ceramics using zircon as a modifying agent. *Ceram. Int.* **2018**, *44*, 19590-19596.
27. Pavlikov, V.M., Garmash, E.P., Yurchenko, V.A., Pleskach, I.V., Oleinik, G.S., Grigor'ev, O.M. Mechanochemical activation of kaolin, pyrophyllite, and talcum and its effect on the synthesis of cordierite and properties of cordierite ceramics. Powder Metall. Met. Ceram. **2011**, *49*, 564-574.
28. Keskin, C.S., Çakır, C.A., Altundağ, H., Toplan, N., Toplan, H.Ö. The effects of mechanical activation on corrosion resistance of cordierite ceramics. *Turk. J. Anal. Chem.* **2023**, *5*, 83-88.
29. Chae, K.W., Son, M.A., Park, S.J., Kim, J.S., Kim, S.H. Effect of sintering atmosphere on the crystallizations, porosity, and thermal expansion coefficient of cordierite honeycomb ceramics. *Ceram. Int.* **2021**, *47*, 19526-19537.
30. Khomenko, O., Zaichuk, A., Amelina, A. Low-temperature cordierite ceramics with porous structure for thermal shock resistance products. Open Ceramics **2024**, *17*, 100520.